Normal and Shear Forces between a Polyelectrolyte Brush and a Solid Surface

NIR KAMPF,[1] JEAN-FRANÇOIS GOHY,[2] ROBERT JÉRÔME,[2] JACOB KLEIN[1,3]

[1]Department of Materials and Interfaces, Weizmann Institute of Science, Rehovot 76100, Israel

[2]Center for Education and Research on Macromolecules, University of Liège, Sart-Tilman B6, 4000 Liège, Belgium

[3]Physical and Theoretical Chemistry Laboratory, Oxford University, South Parks Road, Oxford OX1 3QZ, U.K.

Received 1 July 2004; revised 4 October 2004; accepted 12 October 2004
DOI: 10.1002/polb.20321
Published online in Wiley InterScience (www.interscience.wiley.com).

ABSTRACT: The diblock copolymer poly(methyl methacrylate)-*b*-poly(sodium sulfonated glycidyl methacrylate) (PMMA-*b*-PSGMA) was end-attached by its hydrophobic block (PMMA) onto mica hydrophobized by a stearic trimethylammonium iodide (STAI) layer, to form a polyelectrolyte brush immersed in water. With a surface force balance (SFB), we extended earlier measurements between two such brush layers for the case of normal and shear forces at different shear rates, surface separation, and compressions between one mica surface coated with STAI or a STAI-diblock layer against a bare mica surface. After coating one of the surfaces with STAI, a long range attraction that results in a jump into an adhesive flat contact between the hydrophobic and hydrophilic surfaces was observed. A very different behavior was seen after forming the polyelectrolyte brush on the STAI-coated surface. The long range attraction was replaced by repulsion, accompanied by very low friction during shear (ca. three orders of magnitude lower than with adsorbed polyelectrolytes). On further compression, a weak attraction to the adhesive contact was observed. From the final surface–surface contact separation, we deduce that most of the polyelectrolyte diblock brush layer was squeezed out from the gap, leaving the STAI layer and a small amount of the polymer attached to the surface. Stick-sliding behavior was seen while applying shear, suggesting a dissipation mechanism caused by the trapped polyelectrolyte. J Polym Sci Part B: Polym Phys 43: 193–204, 2005
Keywords: polyelectrolyte brushes; lubrication; diblock copolymers; surfactants

INTRODUCTION

Over the last decade there have been many reports on normal and shear forces between surfaces bearing polymeric brushes. In particular, polyelectrolyte (PE) brush monolayers have recently received considerable interest because of their possible relevance to lubrication in biological systems[1,2] that occur between cells, tissues, and organs in various organisms. One can define biolubrication as the mechanism of reducing friction between biological cells or tissues. This mechanism can involve lubricating fluids composed of natural polymers such as hyaluronic acid, present in the synovial fluid.[3–5] These molecules are secreted from the cells into the extracellular matrix. Molecular layers with a biological affinity can also serve for

Contribution from the February 2004 Meeting of the American Physical Society—Division of Polymer Physics, Montreal, Canada

Correspondence to: J. Klein (E-mail: jacob.klein@weizmann.ac.il or jacob.klein@chem.ox.ac.uk)

Journal of Polymer Science: Part B: Polymer Physics, Vol. 43, 193–204 (2005)

biolubrication and biocompatibilization of artificial implants by mimicking biologically identical interfacial properties.[6]

Many experimental and theoretical studies on the interaction between symmetric PE brushes systems have been performed.[2,7–11] Direct force measurements between such systems were investigated in the past with surface force techniques.[1,12] On the other hand, measurements of normal and shear forces between asymmetric systems composed of polymer brushes versus bare surfaces with such techniques are scarcely reported. Recently, Ohsedo et al.[13] measured the friction forces between gel-terminated PE brushes and a glass plate across water. They found a strong correlation between PE lengths and the measured friction. A low friction coefficient was found for short PE brushes, whereas longer PE molecules exhibited even higher friction than that of a normal network gel at a high sliding velocity. Sheth et al.[14] measured the normal forces between poly(ethylene glycol) (PEG) brushes against various surfaces. They found that the brush did not adhere to a neutral lipid bilayer or to bare mica. However, shear or frictional forces were not mentioned in these studies.[14]

In previous work,[1] we demonstrated that extremely low friction could be attained between surface-bearing symmetric PE brushes across aqueous solutions. In this study we extend this work to the asymmetric case by measuring the normal and shear forces between one surface with a PE brush and another bare charged surface in an aqueous solution.

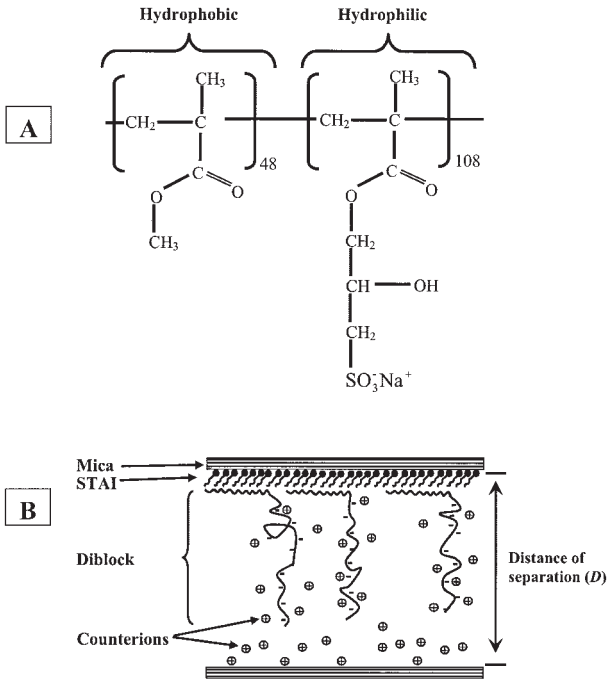

Figure 1. (A) Chemical structure of PMMA-*b*-PSGMA copolymer used in our experiments. (B) Schematic representation (not to scale) of a hydrophobically anchored PE on an STAI-hydrophobized mica surface and their positioning during the force measurements.

EXPERIMENTAL

Materials

Atomically smooth mica sheets (ruby muscovite, grade 1, S & J Trading, Inc., NY) with a thickness of about 1–3 μm were cleaved, half-silvered on one side, and kept under low humidity conditions to prevent oxidation of the silver layer before an experiment. Two half-silvered mica sheets from the same crystallographic primary facet were then glued to a plano/cylindrical fused silica lense (radius 1 cm) with epoxy resin (EPON 1004, Shell Chemicals). The mica-coated lenses were mounted in the surface force balance (SFB) facing each other in a crossed-cylinder configuration, equivalent to the geometry of a sphere over a flat.

Stearic trimethylammonium iodide (STAI: $CH_3(CH_2)_{17}N^+(CH_3)_3I^-$) was kindly synthesized by Dr. J. Frey (Weizmann Institute of Science) according to known methods.[15,16] The surfactant was crystallized twice from a methanol–acetone mixture and an NMR analysis confirmed the elemental composition. Poly(methyl methacrylate)-*block*-poly(sodium sulfonated glycidyl methacrylate) copolymer, from here on referred to as PMMA-*b*-PSGMA or as the diblock, was anionically synthesized and characterized, as reported in detail elsewhere.[12,17–19] The copolymer structure is shown in Figure 1(A) and it is composed of hydrophobic (PMMA)–hydrophilic (polyelectrolytic) (PSGMA) diblocks. It was analyzed by size exclusion chromatography (SEC) and proton nuclear magnetic resonance (^{1}H NMR) for its characteristic molecular features.[19] For the PMMA block, the number of monomers in the hydrophobic chain is 48, and for the copolymer, the number of monomers in the hydrophilic chain is 108.

The copolymer structure is shown in Figure 1(A) and is composed of hydrophobic (PMMA)–hydrophilic (polyelectrolytic) (PSGMA) blocks. It was synthesized by sequential living anionic po-

lymerization of methyl methacrylate (MMA) and glycidylmethacrylate (GMA) as described elsewhere,[19] and it was analyzed by SEC and ^{1}H NMR for its molecular characteristic features. SEC was carried out in tetrahydrofuran (THF) with a Hewlett-Packard 1050 liquid chromatograph equipped with two photoluminescence (PL) gel columns (1000 and 10,000 Å, respectively) and a Hewlett-Packard 1047A refractive index detector. PMMA standards were used for calibration. ^{1}H NMR spectra were recorded at 400 MhZ with a Bruker AM 400 spectrometer. After polymerization of the first block of PMMA, an aliquot was withdrawn from the polymerization medium and analyzed by SEC. The number-average molecular weight (M_n) and the polydispersity [weight-average molecular weight (M_w)/M_n] (1.05) of the PMMA block were then determined and the average number of MMA units in the PMMA block was accordingly calculated to be 48. The second monomer (GMA) was then polymerized and the resulting diblock (PMMA-*b*-PGMA)was analyzed by SEC to determine the M_w/M_n (1.1). The average number of GMA units (108) was calculated from the composition of the PMMA-*b*-PGMA diblock as determined from ^{1}H NMR and from the M_n of the first PMMA block. The PMMA-*b*-PGMA diblock was then converted into the PMMA-*b*-PSGMA diblock by a postsulfonation reaction as described in reference 19. After sulfonation, the PMMA-*b*-PSGMA was dissolved in water and purified by dialysis against regularly replaced bidistilled water for 2 days (Spectra-Por membranes with a molecular weight cutoff of 6000 Da). The degree of sulfonation was then determined by acid–base titration and found to be $\phi = 70\%$. As a result, the number of sulfonate groups in the diblock is Ns = 75 and the molecular weight of the PMMA-*b*-PSGMA copolymer is calculated to be about 30,000.

The charge of the polymer is independent of the local pH because the ionizable groups are sulfonate groups (SO_3^-) that are strong acids.[11] The copolymer was deoxygenated and purified by dialysis against regularly replaced distilled water (Spectra-Por membranes, cutoff 10,000 Da). The PMMA-*b*-PSGMA molecule behaves as a self-associating macrosurfactant with a critical micelle concentration (CMC) of about 1.0 ± 0.2 g/L, as determined by surface tension measurement and dynamic light scattering measurements.[19] Our solutions were far below this concentration.

Ultrapure (conductivity) water was obtained by filtering deionized water with a 5 μm Aquapure® water filter (CUNO, CT), a resin-bonded cellulose filter cartridge (USFilters, PA), and activated charcoal, followed by a Millipore water purification system consisting of a RiOs™ and a MILLI-Q® Gradient A10 stage. The specific resistivity of the water was higher than 18.2 MΩ cm, with a typical pH value in the range of 6.0–6.2. The total organic compound concentration (TOC) was 3–4 ppb or less (as indicated by the A10 TOC measurement unit).

Apparatus

The surface force balance (SFB) used in our experiment was similar to that described by Klein and Kumacheva,[20] and is shown schematically in the inset of Figure 2. White-light multiple beam interferometry enables measurement of the distance D between the mica surfaces (to ±0.2–0.3 nm), and the geometry of the contact region (including the mean radius of curvature of the mica surface $R \approx 1$ cm) to be determined.

The lower surface is mounted on a horizontal leaf spring (spring constant $k_n = 150$ N/m), whose bending, ΔD, is measured by interferometry to yield the normal forces, $F_n(D)$, with a sensitivity of ±50 nN. The upper surface is mounted on a four-sectored (+ 1 internal sector) piezoelectric tube (PZT) (type Pz29, Ferroperm, Denmark). Shear forces, $F_s(D)$, between the surfaces as the upper one is made to move laterally past the lower (in triangular waveform) one are monitored via the bending of a set of vertical springs (spring constant $k_s = 300$ N/m) on which the sectored PZT is mounted, determined via changes in an air gap capacitance (Accumeasure ASP-1-ILA, MTI Instruments, NY). This bending $\Delta X(t)$ of the vertical spring is measured to an accuracy of about ±0.2 nm, to yield the shear force as $F_s(D) = k_s\, \Delta X(t)$.

To minimize ambient vibrations, an electronic vibration isolation system (Halcyonics, MOD-1L, Gottingen, Germany) was used. The noise level in these experiments was higher than reported in some earlier experiments, corresponding to noise in the shear force of about ±0.5–1.0 μN before signal processing. The circuitry of the air gap capacitor may also introduce some high-frequency electronic noise. To improve the signal to noise ratio, the shear traces were frequency-analyzed (fast Fourier transformed, FFT) and the amplitude of signal at the applied frequency was determined, both with the surfaces far apart and at progressively smaller separations. Following subtraction of the systematic error (arising from

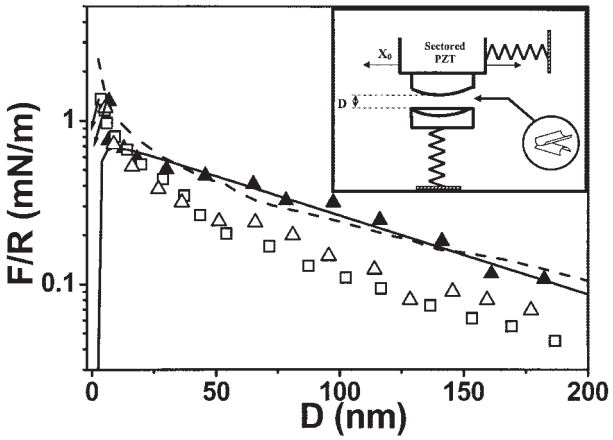

Figure 2. Force [$F_n(D)$] versus distance (D) profiles between mica surfaces across conductivity water normalized as $F_n(D)/R$ in the Derjaguin approximation, where R is the mean radius of curvature of the surfaces (triangles for the first approach). The zero of separation is with respect to contact in water. The solid lines are the theoretical Derjaguin-Landau-Verwey-Overbeek (DLVO) fit to the $F_n(D)/R$ data. The fit corresponds to a Debye length (κ^{-1}) of 90 ± 20 nm [equivalent to an ion concentration of $C = 1(\pm 0.1) \times 10^{-5}$ M], the effective surface charge (σ_0) of one electron per 49.7 nm^2, and the effective surface potential (Ψ_0), found to be −143 ± 20 mV. The jump-in into adhesive flat contact (D = 0.0 ± 0.3 nm) occurs when the surfaces approach about 3 nm. This is probably because of the condensation of the hydrated proton counterions into the charged surface lattice sites, so that van der Waals attraction becomes dominant.[21] For the successive approaches (squares and circles) the $F_n(D)/R$ values in conductivity water may be slightly low, for reasons discussed in ref. 23 (dashed line). Inset—schematic illustration of the surface force balance equivalent to the actual lens/spring assembly used in our experimental setup.[20,22]

coupling of the springs to the apparatus via the thin PZT connection wires), it was found that the sensitivity of the shear force measurements, δF_s, corresponding to the scatter of the shear response at the applied frequency, was about 30 nN.

All glassware and metal tools were first treated with a UV lamp for 30 min to degrade any organic residuals attached to the surfaces. Next, the glassware was cleaned in a piranha solution (H_2SO_4:H_2O_2, 3:1) for about 60 min, then rinsed and sonicated with pure deionized water for 30 min. This cleaned glassware was then rinsed thoroughly with pure conductivity water, filtered analytical grade ethanol, and dried with a Class 100 Laminar Flow Cabinet (Haroshet, Ltd., Israel). After UV treatment, the metal tools were further rinsed and sonicated in toluene, ethanol, pure conductivity water, finally rinsed in ethanol, and left to dry. Until further use, the glassware and metal tools were stored in a laminar flow cabinet.

Procedure

Calibration of the zero separation (D = 0) between the two mica sheets was measured by bringing them into adhesive contact, first in air (43% RH, 24 ± 1 °C), then after introducing conductivity water. Only experiments indicating the absence of contaminants by a typical jump-in to adhesive contact (Fig. 2 and detailed discussion in the RESULTS AND DISCUSSION section) were continued for the STAI coating and subsequent force and shear measurements. Further indication of the purity of the system was given by the absence of a shear response as the surfaces slid past each other, until a jump-in to adhesive contact occurred.

Hydrophobizing the Mica Surface

After calibration in air and conductivity water, only the upper mica surface was removed from the SFB in a clean environment and working conditions, and the mica surface was coated with STAI according to the well characterized and established method.[1,16] After assembly of the STAI layer and rinsing in excess water, the surface was visually inspected for its dryness. The efficiency of the hydrophobization process was also monitored by contact angle measurements (see below).

Assembly of the PE Brushes on Mica

The STAI-coated mica was incubated for about 13 ± 1 h in a 0.3 μM diblock solution outside the SFB. While the upper surface was incubating in the diblock solution, the lower mica surface glued on its lens was immersed in conductivity water in the sealed SFB. After incubation and self-assembly of the PE brush, the upper lens was gently taken out with clean tweezers and rinsed in excess conductivity water (25 °C) for 30 s. The lens coated with STAI and the diblock was then placed back in the SFB, maintaining, as far as possible, the original relative orientation of the surface as that before the upper lens was first removed (a small error in the measurement of the absolute surface D (in the order of a few Å) resulted from a

repositioning mismatch relative to the original orientation.

In this experiment the configuration is different from that of earlier studies[1] that used a similar PMMA-*b*-PSGMA diblock where the PE brushes were attached on both mica sheets within the SFB container. In this experiment, however, removal of excess diblock material from the PE-covered surface ensured that the PE brush on one surface interacted with the bare mica of the other surface across the conductivity water.

Contact Angle Measurement

Contact angle measurements (with an MRL C.A. Goniometer Model 100-00, Rame–Hart, Inc., NJ, connected to a computer and image analysis software) were conducted as a control for the efficiency of the STAI and the PMMA-*b*-PGMAS diblock deposition process. The control contact angle measured on freshly cleaved mica gave $\theta = 2 \pm 1°$, in agreement with previous reports.[14] Coating of freshly-cleaved mica by STAI and by PMMA-*b*-PGMAS was carried out within a laminar flow hood environment, and samples were kept in clean covered vials until contact angle measurement.

Results shown are from three different experiments (different pairs of mica sheets), with data also taken from different contact positions between the mica surfaces in each experiment.

RESULTS AND DISCUSSION

Control Measurements

To ensure cleanliness and integrity of our system, we first confirmed the form of normal surface force between the bare mica surfaces in water. Following air-controls, conductivity water was added to the SFB, and the long-range repulsion between the surfaces (Fig. 2) was followed by a jump-in to adhesive contact from separations Dj = about 4 ± 1 nm, to a contact separation (determining the zero of the surface separation) of -1 ± 0.2 nm relative to air contact. We assume that this is because of the desorption of a thin air-adsorbed contaminant layer of a few Å on each surface and is in line with earlier work.[21,22] Only experiments exhibiting such jumps into contact were considered clean and were continued. A fit with the DLVO model gave the following values for the Debye and surface potential on first approach: $\kappa^{-1} = 90 \pm 20$ nm, corresponding to an ion concentration of $C = 1(\pm 0.1) \times 10^{-5}$ M and a surface potential of -143 ± 20 mV (giving a surface charge density of 1 e/49.7 nm^2). On a second subsequent approach, a somewhat weaker repulsion was observed (Fig. 2), in line with earlier studies[23] (depending on the time elapsed between the profiles). The pull-off force measured on separation yielded an interfacial surface tension of $\gamma = -5.3 \pm 1.7$, via the Johnson-Kendall-Roberts (JKR) relation. This is in line with the range of the reported literature values.[24]

Before the formation of a polyelectrolyte brush layer, we measured the interactions between one STAI layer versus bare mica across water. It has been shown previously with X-ray photoelectron spectroscopy (XPS) that the STAI molecules are preferably attached to the negatively charged mica via the ammonium residue, forming a compact layer with a thickness of 1.0 ± 0.2 nm.[16] The charge distribution on the mica surface is one negative charge per 0.49 nm^2, and from the XPS measurements it seems that most of the charged sites on the mica are occupied by one surfactant molecule.[25]

Normalized force versus distance curves of one-sided STAI-coated mica versus bare mica across pure conductivity water are presented in Figure 3. During the approach, zero forces were recorded within the scatter ($F_n = \pm 35$ μN/m) at a separation $D > 150 \pm 50$ nm. On a closer approach attractive forces were observed, increasing progressively until the surfaces jumped in spontaneously to adhesive contact. The relatively large scatter comes from the nature of the manual distance measurement, hence, the last data point before the jump is in some cases missed. This jump distance was found to be somewhat larger than that reported for two approaching STAI layers across water. Air bubbles on hydrophobic surfaces have been suggested[26,27] as the cause of some long-range hydrophobic attraction, but we saw no evidence of such thin structures on our bare mica in water [atomic force microscopy (AFM) micrographs, not shown here]. The most notable observation was the apparent absence of the long-range osmotic repulsion one might expect because of the single charged mica surface (Figure 3, cartoon inset) that, just before jump-in, should be (from Fig. 2) some 100–200 μN/m. Presumably, this is swamped by the hydrophobic attraction setting before the jump-in.

The characteristics of the adhesive contact between STAI-coated and bare mica surfaces across

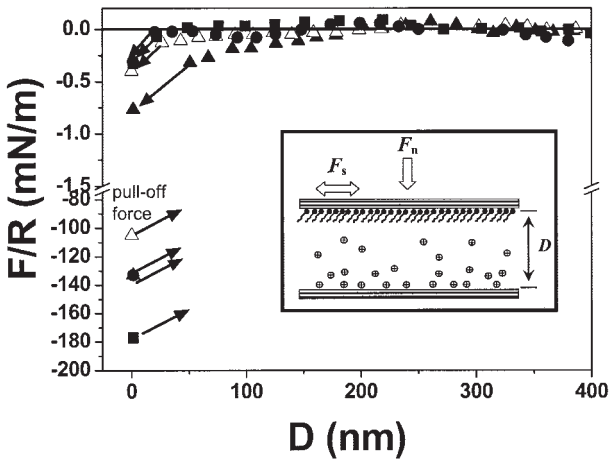

Figure 3. Normalized $F_n(D)/R$ versus distance (D) profiles between STAI against a bare mica surface across conductivity water. Attraction between the surfaces starts at $D < 150 \pm 50$ nm and jumped (indicated by arrows) from $Dj = 33 \pm 14$ nm into flat contact. Filled symbols indicate results measured from first approaches, open symbols indicate results measured from successive approaches, other symbols indicate results from separate experiments. The pull-off adhesion forces are measured from the jump-out distance with the following relation:
$F_{\text{pull-off}} = k \times D$, where k is the normal spring constant, and are presented as the corresponding approach symbols. Inset: schematic representation of STAI layers against bare mica across conductivity water.

conductivity water are presented in Table 1. The distance between one STAI layer and bare mica in the presence of water was found to be $D_o^{STAI} = 1.4 \pm 0.3$ nm. This value is in agreement with the previous XPS and SFB experiments.[16,25] The attachment of the mica charges to the STAI molecule is via the trimethylammonium ion head group. Its cross-section is larger than that of the rest of the C18-alkyl chain, thus, the chains are likely to be tilted to maximize van-der-Waals (vdW) interactions between the alkyl chains. The conformation of the C18 molecule on mica was recently studied with molecular dynamic simulations.[28,29] It was proposed that to optimize the van der Waals interactions, the inclination angle of the C18 molecules on the mica sheet is 55° from the normal plane, at 20 °C. This means that the overall packed hydrophobic layer thickness should decrease by about 30% from its fully stretched length. This value fit into our experimental results that instead of about a 2.5 nm layer thickness between the STAI to bare mica surface in the presence of water, we determined a value of 1.4 nm.

Shear measurements between the approaching covered STAI and lower mica revealed no shear between them (ca. the noise level) as the top surface moved back and forth laterally past the lower one, up to the point where they spontaneously jumped into contact. After adhesive contact, the surfaces were rigidly coupled and moved in tandem over the range of lateral motion applied. From the final D_o^{STAI} we concluded that there is no evidence whatever of any water or water vapor or of any other material between the STAI layer and the bare mica in this adhesive contact. This indirect evidence is in line with earlier studies.[30] From the pull-off force, an effective work of adhesion was evaluated that was some 30–35% lower than for the two interacting STAI surfaces.

Contact Angle Measurements

To monitor the adsorption dynamics of the diblock onto the mica surface, contact angle measurements of pure conductivity water drops were car-

Table 1. Characteristics of the Contact between Bare or Brush-Coated Surfaces Across Conductivity Water

	*D_0 (nm)	Pull-off Force (mN)	Interfacial Tension (mN/m)
Bare mica in humid air	1.0 ± 0.2	—	—
Bare mica in water	0.0 ± 0.3	0.4 ± 0.1	5.3 ± 1.7
Bare mica vs. STAI in water	1.4 ± 0.3	1.1 ± 0.1	13.0 ± 1.1
Bare mica vs STAI-PMMA-*b*-PSGMA in water	2.9 ± 0.1 (1.7 ± 0.1#)	0.19 ± 0.04	2.2 ± 0.4
STAI vs STAI in water	2.1 ± 0.4	1.6 ± 0.1	19.5 ± 1.9
STAI vs. STAI-PMMA-*b*-PSGMA in water	3.2 ± 0.1	0.6 ± 0.1	7.0 ± 1.5

* Relative to mica-mica contact in conductivity water.
# Measured in the first approaches.

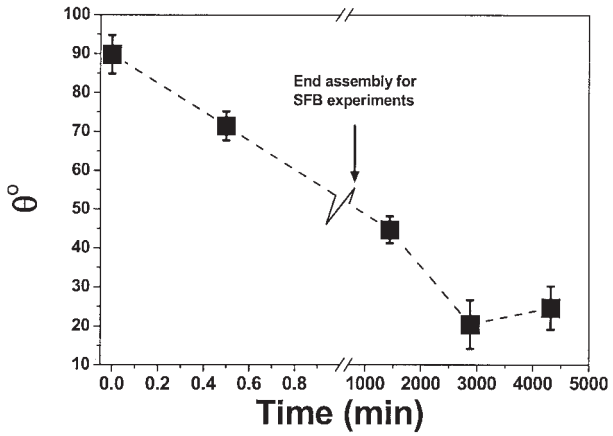

Figure 4. Contact angle measurements of pure conductivity water drops on STAI–PMMA-*b*-PGMAS diblock coated mica at different assembly times. The contact angle of conductivity water on bare mica was $\theta = 2 \pm 1°$. Results shown at time $t = 0$ correspond to the contact angle of water on STAI coated mica. For $t > 0$ the results referred to the self assembly process of the PMMA-*b*-PGMAS diblock on the hyhdrophobized mica.

ried out on STAI-coated mica and STAI–PMMA-*b*-PGMAS diblock coated mica following different periods of self-assembly of the layers (Fig. 4). The average contact angle between STAI coated mica and pure water was found to be $\theta = 89.8 \pm 5°$. This value was found to be slightly higher than in previous reports (80–85°),[16,25] possibly because of a minor change in the working conditions and surface coverage. Our results indicate that because the surfaces were dry after the coating process, most of the negatively charged sites on the mica were occupied by the STAI molecules. No change of the contact angle was observed at different deposition or storage times (up to three days) for the STAI layer on the mica in pure conductivity water.

A rapid decrease to about 30% of the contact angle of the hydrophobic layer was observed after immersion of the STAI-coated mica into a PMMA-*b*-PGMAS diblock solution for the first 30 s. The reduction in contact angle was continued but at a somewhat slower rate and reached a steady state after about 46 h. After about three days the contact angle remained at 25% of its initial value. The general phenomenon of reduction in the contact angle is expected because as more hydrophobic moieties are attached to the STAI-coated mica, the more hydrophilic tails of the polyelectrolyte are exposed to the interface.

For the SFB experiments, we have chosen a partially diblock covered surface and the self-assembly process was stopped after 13 ± 1 h because the lower mica surface immersed in pure water in the SFB is prone to water-soluble contaminants if it is exposed unprotected for excessively long periods of time. Refractive index measurements on similar confined PE layers[1] revealed an adsorbance of $\Gamma = 3 \pm 1$ mg/m^2, corresponding to a mean surface spacing between chains of 4 ± 0.7 nm. Taking into consideration the PE cross-section area (roughly about 1 nm), it can be suggested that after 12–13 h of self-assembly, the surface is partially occupied by the PE brush.

Polyelectrolyte Brush versus Bare Mica

Following controls between the bare mica surfaces across water and the preparation of the PE brush on the top surface as described earlier, the normal interactions were long-range and repulsive, as shown in Figure 5. The PSGMA can be termed as a *strong* polyelectrolyte brush because

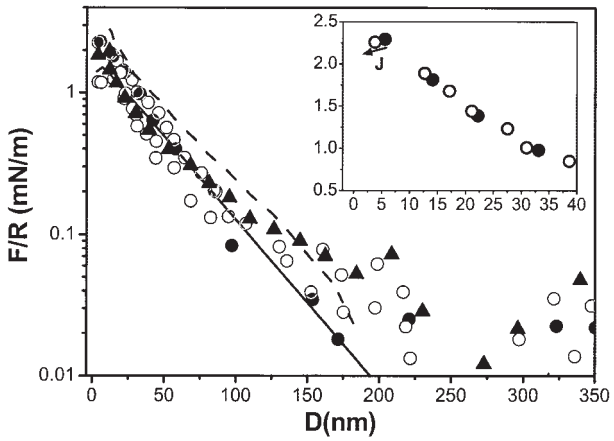

Figure 5. Normalized $F_n(D)/R$ versus distance (D) profiles between a PE brush PMMA-*b*-PSGMA versus a bare mica surface across conductivity water. Filled symbols indicate results measured from first approaches, open symbols indicate results measured from successive approaches, different symbols indicate results from separate experiments. Data was fitted with DLVO theory (solid line), with a Debye length of $\kappa^{-1} = 35 \pm 3$ nm, corresponding to an ion concentration of $C = 7.5 \pm 1.5 \times 10^{-5}$ M. The dashed guideline indicates the results from Ref. 1. Inset: normal force profile profiles between PMMA-*b*-PSGMA polyelectrolyte brushes versus bare a mica surface across conductivity water from 40 nm down to contact. The jump (J) into adhesive contact from $D = 4 \pm 1$ nm to $D_0^{\text{diblock}} = 2.9 \pm 0.1$ nm (1.7 ± 0.1 nm for the first approach) is indicated by an arrow.

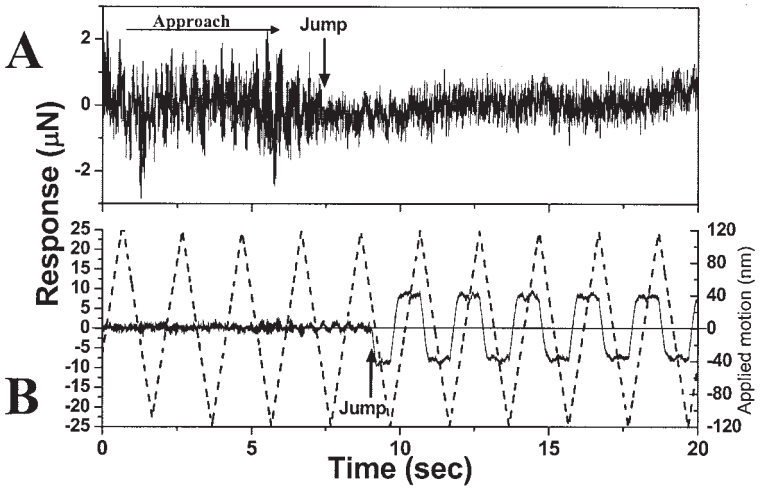

Figure 6. (A) The jump event between the PE brush against bare mica and across conductivity water during the approach between surfaces driven by thermal drift (R_d = 0.7 ± 0.2 nm/s), as was evident by ambient natural noise reduction recorded in the oscilloscope. (B) The approach driven by thermal drift during applied shear (V_s = ca. 300 nm/s indicated by the dashed trace) between the PE brush against bare mica across conductivity water. The response to shear after the surfaces came into adhesive contact is evident by stick-sliding behavior.

the number and position of charges in the chain is fixed.[2,7] We note that significant repulsive forces start below 150 nm and monotonically increased down to few nm. The forces during compression were slightly lower (by somewhat more than the scatter in the data) than the measured force profiles reported for the two opposed PMMA-*b*-PSGMA surfaces[1] (as indicated by the dashed line in Fig. 5), and the unperturbed thickness, L, of a similar PE brush layer was estimated in this work as 13 ± 2 nm.

The Debye length was calculated by fitting the far-field data ($D > 50$ nm, outside the range of expected steric interactions because of the extended brush) to DLVO theory, and found to be about 35 nm, corresponding to an ion concentration of $C = 7.5 \times 10^{-5}$ M. This suggests the presence of additional counterions in the brush/bare-mica gap relative to the bare-mica/bare-mica gap. This may arise from the brush-layer itself. However, the application of the DLVO model that developed for the forces between two well-defined charge-bearing surfaces[31] to the case of one surface interacting with a diffuse PE brush layer and its associated charge distribution is clearly an approximation.

The form of repulsive interaction is complicated, and it is difficult to attach a quantitative significance to it. Qualitatively, it seems that the initial repulsion (250 nm $< D <$ 75 nm) has a larger decay length, suggesting a counterion concentration in the brush/bare-mica gap similar to that in free water (Fig. 2). Because force measurements were performed across pure water, one can assume that the PE is stretched and the interactions within and between the charged chains are repulsive. This is known to form an extended conformation of the brush.[2,7] As the surfaces further approach, the repulsion increases more rapidly, suggesting the influence of a higher counterion concentration in the gap, possibly because of ions from the brush-layer itself. Finally, at $D \leq 20$ nm, the rise in repulsive force may reflect steric interactions because of the brush chains (whose fully-extended length is about 30 nm) being pressed against the mica.

For compression higher than about 2500 μN/m, there is some indication of a weak jump into adhesive contact, from D = about 4 ± 1 nm to D = 1.7 ± 0.3 nm (Fig. 5, inset). The jump event was also evidenced by an ambient natural noise reduction recorded in the oscilloscope (trace A in Fig. 6). This is probably because of the expulsion of most of the diblock from between the surfaces, leaving a residual (probably flattened) PE layer with a thickness of about 0.5 nm. The adhesion between the surfaces (Table 1) is much weaker than for STAI on bare mica (Fig. 3 and Table 1), and does not lead to flattening of the supportive glue (as in the case for mica–mica,[21] mica-STAI,

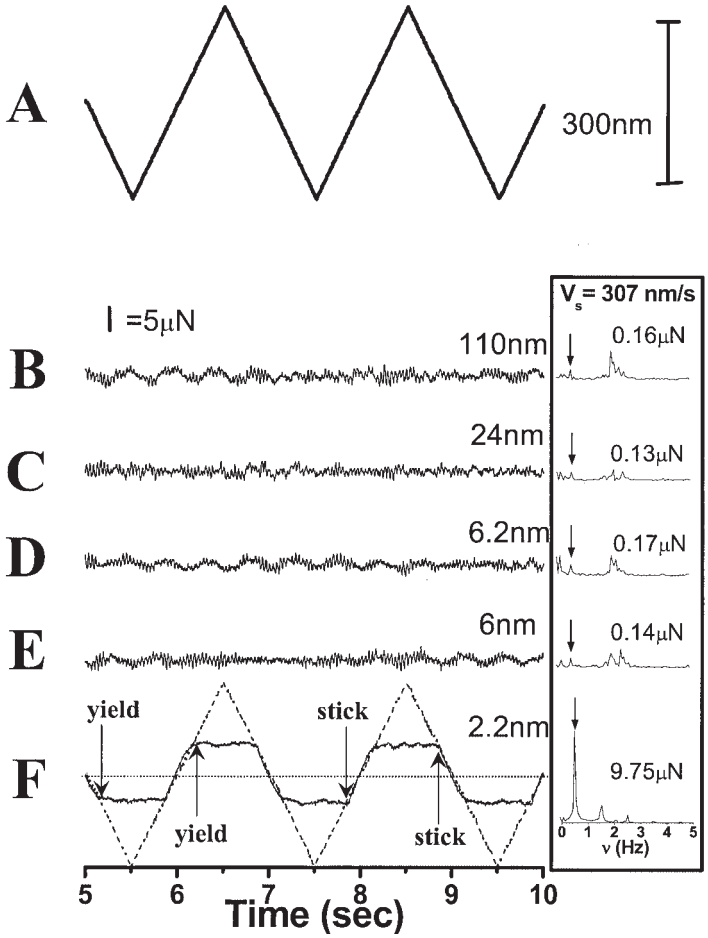

Figure 7. As-recorded oscilloscope traces from shear measurements: Trace A: applied back-and-forth motion to upper surface (amplitude of applied motion versus time); traces B–F: shear forces transmitted between the surface bearing a PE brush and a bare mica surface at different surface separations, D, as indicated in response to applied motion n trace A. The right hand traces are the frequency dependent shear forces determined by FFTs of traces B–F. The dashed line in trace F is the shear response (at the same V_s as applied on the corresponding PE brush) between hydrophobized mica by the STAI layer versus bare mica in adhesive contact, as demonstrated in the control experiment (Fig. 3). The dotted line in trace F represents the mid-shear position ($\Delta X_s = 0$) position of the PZT. The stick and yield points between the PE brush and bare mica at contact are indicated by arrows.

and STAI–STAI[25] adhesive contacts). The shear force variation as the surfaces approach under a thermal drift is shown in Figure 6, both for the case of no applied lateral shear [Fig. 6(A)], and when shear was applied. In the latter case, the situation proceeds from an absence of detectable shear force, with no intermediate stage, abruptly to one where the friction is high (although, because of the residual PE chains, lower than for STAI/bare-mica contact).

Shear force measurements between STAI–PMMA-*b*-PGMAS coated mica versus bare mica in the presence of conductivity water were carried out by applying back-and-forth lateral motion to the top polymer-coated surface with respect to the lower surface. The measurements commenced at large surface separations ($D > 100$ nm) where no normal forces above the scatter could be observed, and typical as-recorded shear-force traces are shown in Figure 7. Trace A in Figure 6 shows the shear motion $\Delta X_0(t)$ applied to the upper surface as a function of time, whereas traces B–F are the corresponding shear forces $F_s(t)$ transmitted across the gap between them at different surface

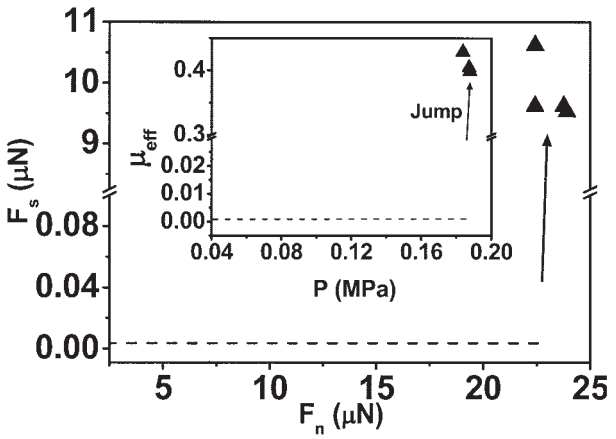

Figure 8. Shear forces (F_s) measured at different normal forces (F_n) between a PMMA-*b*-PSGMA polyelectrolyte brush against bare mica surface across conductivity water. The baseline shear force after subtraction of the natural ambient noise is indicated as a dashed line. Inset. Variation of the effective friction coefficient, μ_{eff}, with increasing surface pressure. Different data points were taken from various sets of experiments. The jump into adhesive contact is indicated by an arrow.

separations, as shown. The right hand side of the traces shows the shear force components as a function of frequency (derived from the FFT analysis of the traces), with an arrow indicating the drive frequency ω_0 (0.5 Hz). Even for the largest separations, trace B in Figure 7, where there is no measurable normal interaction between the surfaces, there is still a residual shear force F_{s0} (ω_0) (in the range of 130–160 nN, varying between different experiments), measurable at the drive frequency over and above the noise level; this arises from the coupling of the upper surface to the lower surface via the thin wires connected to the PZT. This systematic signal (not because of any polymer/polymer interactions) may be subtracted from the actual signal to yield $F_s(D, \omega_0)$, the relevant shear force at the sliding velocity of the measurements, as revealed in traces B–F in Figure 7.

The shear force results showed that down to 6 nm, the magnitude of F_s is on the order of the baseline noise level measured at a far distance (Fig. 8). At this distance (6 nm), estimated from the JKR, the pressure between the surfaces can be calculated as: F_n/A_{eff} (where the effective area, A_{eff}, is $1(\pm 0.1) \times 10^{-10} m^2$) and found to be 1.7 $\pm$ 0.1 atm and the estimated friction coefficient, $\mu_{eff} = F_s/F_n$, has an upper limit of $\mu_{eff} < 5(\pm 2) \times 10^{-3}$ (Fig. 8, inset). This very low friction between the polyelectrolyte–brush and bare charged mica surface was similar to what was observed between the two opposing polymer brush layers,[1] even though in the current study the charged polymer was rubbed against bare mica and not on an opposing polyelectrolyte brush. We attribute this to factors similar to those responsible for the low friction between two interactive PE brushes: adhesion between the brush and the possible presence of fluid hydration sheets near the charged segment that act as molecular ball-bearings.

Supporting evidence for the possible polyelectrolyte residuals (i.e., the trapped PE after the surfaces jumped to an adhesive contact; see above) between the STAI and the bare mica is given by comparing to the shear behavior between rigidly coupled STAI–bare mica surfaces, presented as a dashed line in trace D (Fig. 9) is the shear response [at a shear velocity (V_s) = 307 nm/s). Unlike the case of the STAI–bare mica contact, where the surfaces were rigidly coupled over the applied lateral amplitudes, here we found a stick-slip behavior in the contact probably because of the lubricating action of the residual diblock chains. If the negatively sulfonated charged polymer is oriented parallel to the surface, the negative charges from the mica surface and the polyelectrolyte may repel, facilitating eventual sliding. The picture is one where the STAI–mica adhesion is reduced by the trapped diblock chains that at the same time reduce the friction on sliding.

In Figure 9 the shear force response is shown for a D value of 1.8 nm (contact following removal of most of the diblock on strong compression). It is of interest that at relatively low shear velocities (below about 300 nm/s) the shear response is one of rigid coupling followed by free sliding. At lower shear rates, the response is characteristic of a mixed sliding and spring-bending. This, interestingly, suggests that the effective relaxation rate of the trapped polymer mediating the friction is somewhat in the region of the shear rates corresponding to this transition in behavior. We may roughly estimate that: if the thickness of the sheared residual polymer layer is about 0.5 nm, the relevant shear rate at a shear velocity of 300 nm/s is about 600 s^{-1}, and this is roughly the relaxation rate of the trapped diblocks.

The variation of the shear force with increasing shear velocity (V_s) between PE brushes versus bare mica in contact across conductivity water

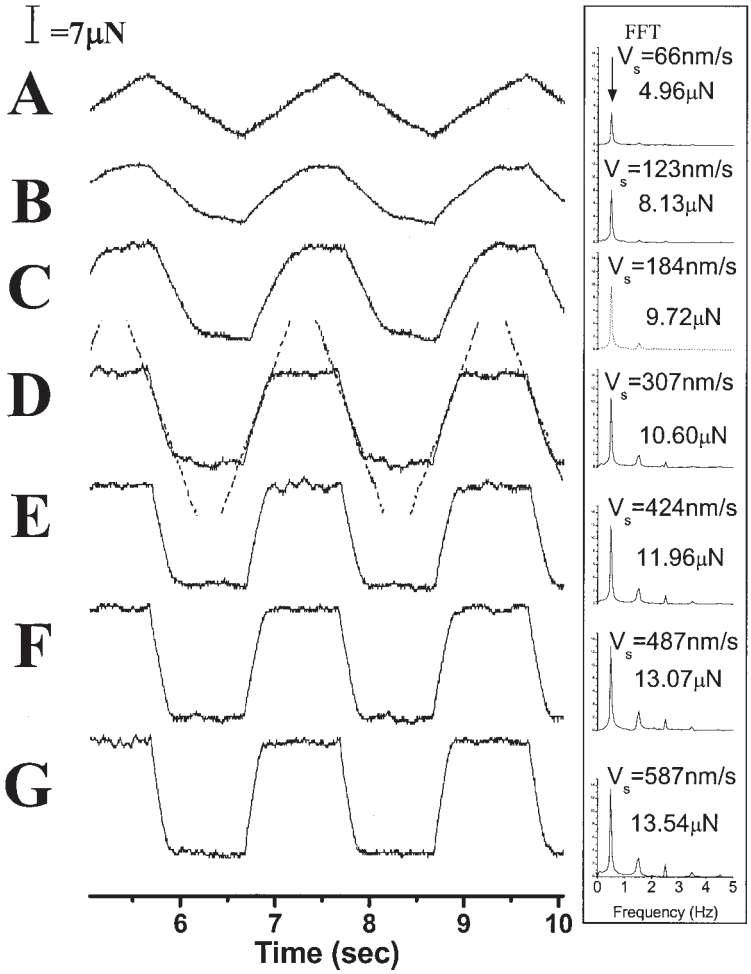

Figure 9. Typical shear traces (traces A to G) applied between a PE brush versus bare mica in conductivity water, taken from the recording oscilloscope at different amplitudes for a particular case (at D = 1.8 nm). The dashed line in trace D is the shear response (V_s = 307 nm/s) between the STAI layer against bare mica in adhesive contact, as demonstrated in the control experiment (Fig. 3). Right inset: frequency-dependent shear forces determined by FFT from traces A to F.

was measured in different experiments and at contact points and is presented in Figure 10. There is a large variation between different experiments, suggesting a considerable variance in the residual amount of diblock after the polymer was squeezed out at high compression. The general trend within a given experiment is that of a dissipative mechanism, somewhat different than that of solid–solid friction, where shear force varies even more weakly—logarithmically—with shear velocities.[20]

CONCLUSIONS

A model system composed of PMMA-*b*-PSGMA that end-attached to form a PE brush on a hydrophobic layer (STAI) was used to determine the interaction between such a negatively charged PE brush and bare hydrophilic surfaces across water. During this, we showed that uniform and stable hydrophobic (STAI) surfaces were attracted to highly charged hydrophilic surfaces (bare mica) across salt-free water. We showed that this single charged brush is compressed and slides across the solid surface, and very low friction is maintained (essentially below our detection) until the abrupt removal of most of the polymer from between the surfaces by compression. Although there is no direct evidence for elimination of the brush from the gap, the indirect measurements provided in this study can support such a mechanism. We attribute the ultralow friction to the very fluid

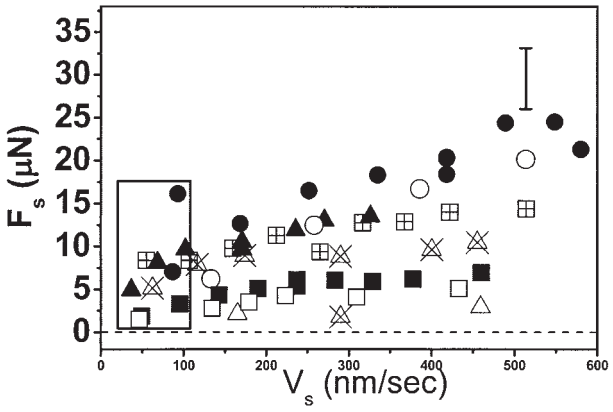

Figure 10. Summary of the yield shear force (F_s) with applied shear velocity (V_s) between a PE brush against bare mica in conductivity water at $D = 2.7 \pm 1.1$ nm and a normal load $F/R = 1850 \pm 250$ μN/m. Data within the box area did not exhibit clear stick-sliding behavior, as demonstrated in trace A of Figure 9. The shear response measurements in contact were taken at different experiment and contact points (different symbols). Filled symbol data points are for the first approach and open symbols are for the second approach at the same contact position.

interface between the brush and the charged solid surface, arising from its nonadhesion to the surface and to hydration layers near the charges on both mica and the polymer brush backbone. Our results extend earlier studies on the reduction of friction by polymeric lubricants, in particular, between two polyelectrolyte brushes. They may have a relevance to biolubrication when charged macromolecules at the surface are ubiquitous.

We appreciate the help of J. Frey for synthesizing the STAI molecule, and we thank U. Raviv for his helpful discussions and M. Omer and T. Pereg for the contact angle measurements.

REFERENCES AND NOTES

1. Raviv, U.; Giasson, S.; Kampf, N.; Gohy, J. F.; Jerome, R.; Klein, J. Nature 2003, 425, 163–165.
2. Ruhe, J.; Ballauff, M.; Biesalski, M.; Dziezok, P.; Grohn, F.; Johannsmann, D.; Houbenov, N.; Hugenberg, N.; Konradi, R.; Minko, S.; Motornov, M.; Netz, R. R.; Schmidt, M.; Seidel, C.; Stamm, M.; Stephan, T.; Usov, D.; Zhang, H. Adv Polym Sci 2004, 165, 79–150.
3. Laurent, T. C. In Interstitum, Connective Tissue and Lymphatics; Reed, R. K.; McHale, N. G.; Bert, J. L.; Winlove, C. P.; Laine, G. A., Eds.; Portland Press: London, 1995, pp 1–12.
4. Albersdorfer, A.; Sackmann, E. Eur Phys J B 1999, 10, 663–672.
5. Hokputsa, S.; Jumel, K.; Alexander, C.; Harding, S. E. Eur Biophys J 2003, 32, 450–456.
6. Tsukruk, V. V. Adv Mater 2001, 13, 95–108.
7. Pincus, P. Macromolecules 1991, 24, 2912–2919.
8. Abe, T.; Higashi, N.; Niwa, M.; Kurihara, K. Langmuir 1999, 15, 7725–7731.
9. Zhulina, E. B.; Wolterink, J. K.; Borisov, O. V. Macromolecules 2000, 33, 4945–4953.
10. Seidel, C. Macromolecules 2003, 36, 2536–2543.
11. Tamashiro, M. N.; Hernandez-Zapata, E.; Schorr, P. A.; Balastre, M.; Tirrell, M.; Pincus, P. J Chem Phys 2001, 115, 1960–1969.
12. Abraham, T.; Giasson, S.; Gohy, J. F.; Jerome, R. Langmuir 2000, 16, 4286–4292.
13. Ohsedo, Y.; Takashina, R.; Gong, J. P.; Osada, Y. Langmuir 2004, 20, 6549–6555.
14. Sheth, S. R.; Efremova, N.; Leckband, D. E. J Phys Chem B 2000, 104, 7652–7662.
15. Kodama, M.; Tsujii, K.; Seki, S. J Phys Chem 1990, 94, 815.
16. Tadmor, R.; Rosensweig, R. E.; Frey, J.; Klein, J. Langmuir 2000, 16, 9117–9120.
17. Leemans, L.; Fayt, R.; Teyssie, P. J Polym Sci Part A: Polym Chem 1990, 28, 1255.
18. Gohy, J. F.; Antoun, S.; Jerome, R. Polymer 2001, 42, 8637–8645.
19. Gohy, J. F.; Antoun, S.; Jerome, R. Polymer 2001, 42, 8637–8645.
20. Klein, J.; Kumacheva, E. J Chem Phys 1998, 108, 6996–7009.
21. Raviv, U.; Laurat, P.; Klein, J. Nature 2001, 413, 51–54.
22. Kampf, N.; Raviv, U.; Klein, J. Macromolecules 2004, 37, 1134–1142.
23. Raviv, U.; Laurat, P.; Klein, J. J Chem Phys 2002, 116, 5167–5172.
24. Pashley, R. M. J. Colloid Interface Sci 1981, 80, 153–162.
25. Raviv, U.; Giasson, S.; Frey, J.; Klein, J. J Phys: Condens Matter 2002, 14, 9275–9283.
26. Zhang, X. H.; Zhang, X. D.; Lou, S. T.; Zhang, Z. X.; Sun, J. L.; Hu, J. Langmuir 2004, 20, 3813–3815.
27. Mao, M.; Zhang, J. H.; Yoon, R. H.; Ducker, W. A. Langmuir 2004, 20, 1843–1849.
28. Heinz, H.; Castelijns, H. J.; Suter, U. W. J Am Chem Soc 2003, 125, 9500–9510.
29. Heinz, H.; Paul, W.; Suter, U. W.; Binder, K. J Chem Phys 2004, 120, 3847–3854.
30. Claesson, P. M.; Herder, P. C.; Blom, C. E.; Ninham, B. W. J Colloid Interface Sci 1987, 118, 68–79.
31. Derjaguin, B. V.; Churaev, N. V.; Muller, V. M. Surface Forces; Plenum: New York, 1987.